Regular Article

PHYSICAL CHEMISTRY RESEARCH
Published by the
Iranian Chemical Society
www.physchemres.org
info@physchemres.org

***Phys. Chem. Res.**, Vol. 3, No. 2, 99-110, June 2015.*
DOI: 10.22036/pcr.2015.7800

Sonochemical Green Method for Preparation of Mg-Doped ZnO Nanostructures in Water with Enhanced Photocatalytic Activity

H. Nouri and A. Habibi-Yangjeh*
Department of Chemistry, Faculty of Sciences, University of Mohaghegh Ardabili, P.O. Box 179, Ardabil, Iran
(Received 20 August 2014, Accepted 14 January 2015)

In this work, Mg-doped ZnO nanostructures were prepared in water under ultrasonic irradiation for 60 min without using any organic compounds or post preparation treatments. The prepared samples were characterized by X-ray diffraction (XRD), scanning electron microscopy (SEM), transmission electron microscopy (TEM), energy dispersive analysis of X-ray (EDX), diffuse reflectance spectroscopy (DRS), and Fourier transform-infrared (FT-IR) techniques. Powder XRD patterns display that ZnO has wurtzite hexagonal crystalline phase and loading of Mg^{2+} ions does not change its crystalline phase. The SEM and TEM images represented that morphology of Mg-doped ZnO nanostructures remarkably is different from the undoped one. Photocatalytic activities of the samples were investigated by degradation of methylene blue under UV irradiation. The degradation rate constant on Mg-doped ZnO nanostructures increases nearly 2.5-fold relative to the undoped one. Influence of various operational parameters, such as ultrasonic irradiation time, calcination temperature, and pH of the solution on the degradation activity was investigated and the results discussed. Finally, the results showed that the holes and hydroxide radicals are the main species in degradation of the pollutant.

Keywords: Mg-doped ZnO, Ultrasonic irradiation, Photocatalysis, Nanostructures

INTRODUCTION

Nanomaterials with the size range of a few nanometers have received considerable attention because of their interesting properties [1-3]. Heterogeneous photocatalysis using nanomaterials of semiconductors is an effective method to destroy a wide range of organic pollutants at ambient temperatures and pressures [4,5]. The initial step of the photocatalytic processes is absorption of photons with a wavelength adequate to match energy levels of photocatalyst to induce electron promotion from the valence band to the conduction band of the photocatalyst and producing electron-hole pairs [6]. The photogenerated pairs are recombined within a time scale of nanoseconds and only small percentage of them migrate to surface of the photocatalyst, where they can be captured by adsorbed molecules to start catalytic reactions [7]. High chemical and thermal stability, low-cost, and nontoxicity are the main reasons for the widespread acceptability of ZnO nanomaterials compared to the other photocatalysts [8]. It is generally known that a major hindrance for enhancing photocatalytic activity is fast recombination of electron-hole pairs [5,6]. Hence, one of the effective strategies to address this problem is to suppress recombination of photogenerated electrons and holes [8].

In recent years, many synthetic methods have been applied for preparation of Mg-doped ZnO nanomaterials, such as rheological phase reaction [9], microwave combustion and microwave polyol [10], wet chemical [11], oxalate coprecipitation [12], sol-gel [13,14], and microwave irradiation [15]. These preparation methods mainly employ harmful chemicals, high temperatures or longer reaction times.

Due to simplicity of the method, low price of the equipment and crystalline phase of the as-prepared samples, utilization of ultrasonic irradiation for preparation of

*Corresponding author. E-mail: ahabibi@uma.ac.ir

different nanomaterials has been a research topic of great interest [16-19]. However, preparation of Mg-doped ZnO nanomaterials using this method and investigation of their photocatalytic activities has been rarely reported. Xiong *et al*. prepared Mg-doped ZnO nanoparticles in tetraethylene glycol by sonochemical method and investigated their photoluminescence activities [20]. Moreover, preparation of Mg-doped ZnO nanoparticles has been reported in diethylene glycol by ultrasonic irradiation method and the prepared samples subsequently heated at 200 °C for 30 min [21]. In these reports, organic solvents have been used and thermal treatment [21] is required. Therefore, it is highly desirable to prepare these nanomaterials by a fast and green method without using any organic solvents and thermal treatments.

Hence, in the present paper, ultrasonic irradiation method was applied for preparation of Mg-doped ZnO nanostructures in water by one-pot procedure without using any organic additives or post preparation treatments. Moreover, photocatalytic activities of the samples were investigated by degradation of methylene blue under UV irradiation. To achieve maximum degradation efficiency, the influence of various operational parameters, such as ultrasonic irradiation time, calcination temperature, weight of catalyst, and pH of solution on the degradation reaction was studied and the results were discussed.

EXPERIMENTAL

Materials

Zinc acetate ($Zn(CH_3COO)_2.2H_2O$, extra pure), magnesium nitrate ($Mg(NO_3)_2.6H_2O$, extra pure), sodium hydroxide, MB, 2-propanol, potassium iodide, benzoquinone and absolute ethanol were obtained from Merck and employed without further purification. Double distilled water was used for the experiments.

Instruments

The ultrasonic irradiation was performed using a Hielscher high intensity ultrasound processor UP200H, Germany (1.4 cm diameter Ti horn, 140 W, 23 kHz). The acoustic power in the solution was 47 W, determined by the heating rate method [22]. X-ray diffraction (XRD) patterns were recorded on a Philips Xpert X-ray diffractometer with Cu Kα radiation (λ = 0.15406 nm). Diffuse reflectance spectra (DRS) were recorded by a Scinco 4100 apparatus. Surface morphology was studied *via* LEO 1430VP scanning electron microscopy (SEM), using an accelerating voltage of 15 kV. The purity of the products was obtained by energy dispersive analysis of X-rays (EDX) on the same SEM. Transmission electron microscope (TEM) measurements were performed on a Philips EM 208 with an acceleration voltage of 100 kV. Fourier transform-infrared (FT-IR) spectra were obtained using Perkin Elmer Spectrum RX I apparatus.

Preparation of the Nanostructures

For preparation of Mg-doped ZnO nanostructures, zinc acetate dihydrate (3.7314 g) and magnesium nitrate hexahydrate (0.7693 g) were dissolved in 100 ml of distilled water under stirring at room temperature. Then, aqueous solution of NaOH (5 M) was dropwise added into the solution under stirring at room temperature until pH of the solution reached to 11. The milky suspension was irradiated in air for 60 min. The formed suspension was centrifuged to get the precipitate out and washed two times with double distilled water and ethanol to remove the unreacted reagents and dried in an oven at 60 °C for 24 h. The schematic diagram for preparation of the nanostructures is illustrated in Scheme 1.

Photocatalysis Experiments

Photocatalysis experiments were performed in a cylindrical Pyrex reactor with about 400 ml capacity. The reactor was provided with water circulation arrangement to maintain the temperature at 25 °C. The solution was magnetically stirred and continuously aerated by a pump to

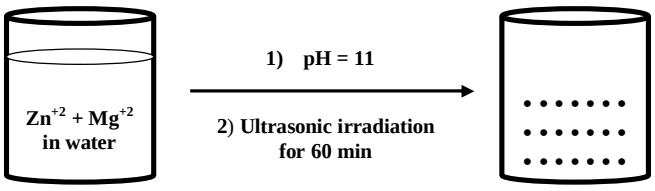

Scheme 1. The schematic diagram for preparation of Mg-doped ZnO nanostructures under ultrasonic irradiation for 60 min.

provide oxygen and complete mixing of the reaction solution. A UV Osram lamp with 125 W was used as UV source. The lamp was fitted on the top of the reactor. Prior to illumination, a suspension containing 0.1 g of the nanostructures and 250 ml of MB (2.75×10^{-5} M) was continuously stirred in the dark for 30 min, to attain adsorption equilibrium. Samples were taken from the reactor at regular intervals and centrifuged to remove the photocatalyst before analysis by spectrophotometer at 664 nm corresponding to maximum absorption wavelength of MB.

RESULTS AND DISCUSSION

The XRD patterns for ZnO nanoparticles and Mg-doped ZnO nanostructures are displayed in Fig. 1. Pure ZnO has diffraction peaks corresponding to (100), (002), (101), (102), (110), (103), (200), (112), (201), (004) and (202) planes in agreement with a wurtzite hexagonal crystalline phase (JCPDS file number of 36-1451) and no other peaks attributable to possible impurities such as $Zn(OH)_2$ are observed [23]. For Mg-doped ZnO nanostructures, the diffraction peaks correspond to ZnO and there are not any diffraction peaks corresponding to impurities such as $Mg(OH)_2$ and MgO. Hence, loading of Mg^{2+} ions does not change ZnO crystalline phase. As clearly seen in Figs. 1b and 1c, for Mg-doped ZnO nanostructures, there are significant changes in peak positions to the higher angles. These shifts are due to the smaller ionic radius of Mg^{2+} (0.66 ´) compared to Zn^{2+} (0.74 ´) [24].

In Figs. 2a and 2b, SEM images for ZnO nanoparticles and Mg-doped ZnO nanostructures are displayed. The undoped ZnO mainly has spherical nanoparticles with diameter of about 60 nm. However, by doping Mg^{2+} ions, morphology of the nanoparticles remarkably changes to highly aggregated nanostructures with different sizes.

The TEM images for ZnO nanoparticles and Mg-doped ZnO nanostructures are shown in Figs. 2c and 2d. It is clear that each grain of ZnO nanoparticles has been composed of highly aggregated smaller particles with the size of about 25 nm. Moreover, morphology of the Mg-doped nanostructures remarkably is different from the ZnO nanoparticles.

Purity of the prepared samples was studied by EDX technique and the results for the undoped and Mg-doped

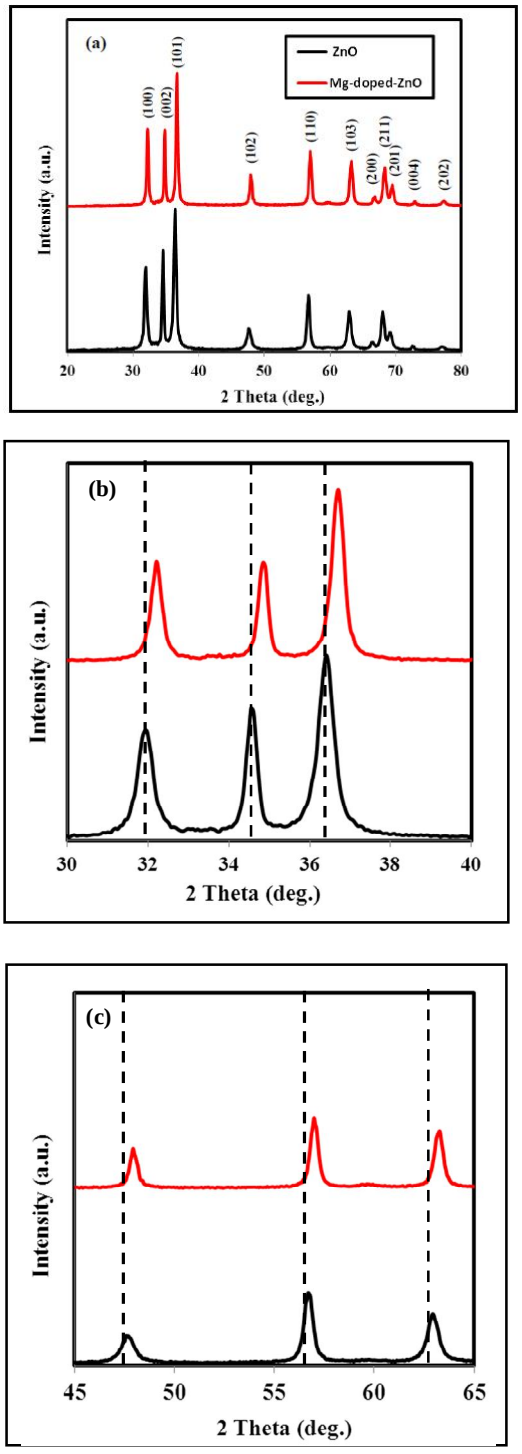

Fig. 1. (a) XRD patterns for ZnO nanoparticles and Mg-doped ZnO nanostructures. (b) and (c) Shifts in XRD pattern of ZnO nanoparticles by doping with Mg^{2+} ions.

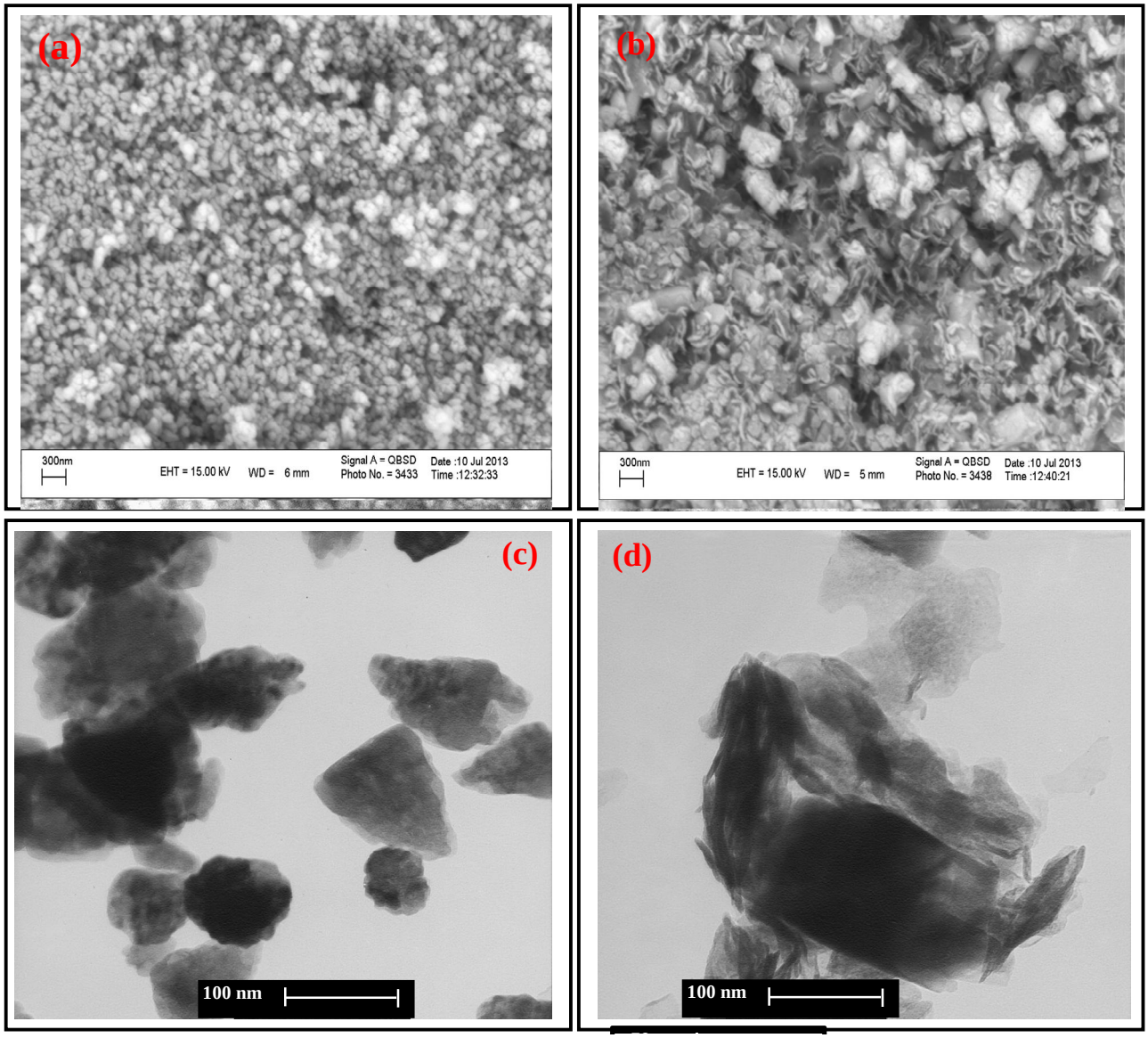

Fig. 2. SEM images for (a) ZnO nanoparticles, (b) Mg-doped ZnO nanostructures. TEM images for (c) ZnO nanoparticles and (d) Mg-doped ZnO nanostructures.

ZnO are shown in Fig. 3. For the undoped ZnO, the peaks are clearly related to Zn and O elements. Moreover, Mg-doped ZnO nanostructures demonstrate the peaks corresponding to Mg along Zn and O elements. Other peaks in these figures correspond to the Au element applied for sputter coating of the samples on the EDX stage.

UV-Vis DRS of the prepared samples was obtained, which the results are shown in Fig. S4a. The pure ZnO has an absorption maximum at about 348 nm. This absorption shows blue shift relative to bulk ZnO with absorption at 384 nm that can be attributed to quantum confinement effect [25]. It reveals that absorption spectrum of Mg-doped ZnO nanostructures is similar to that of the undoped one.

The FT-IR spectra for the undoped and Mg-doped ZnO

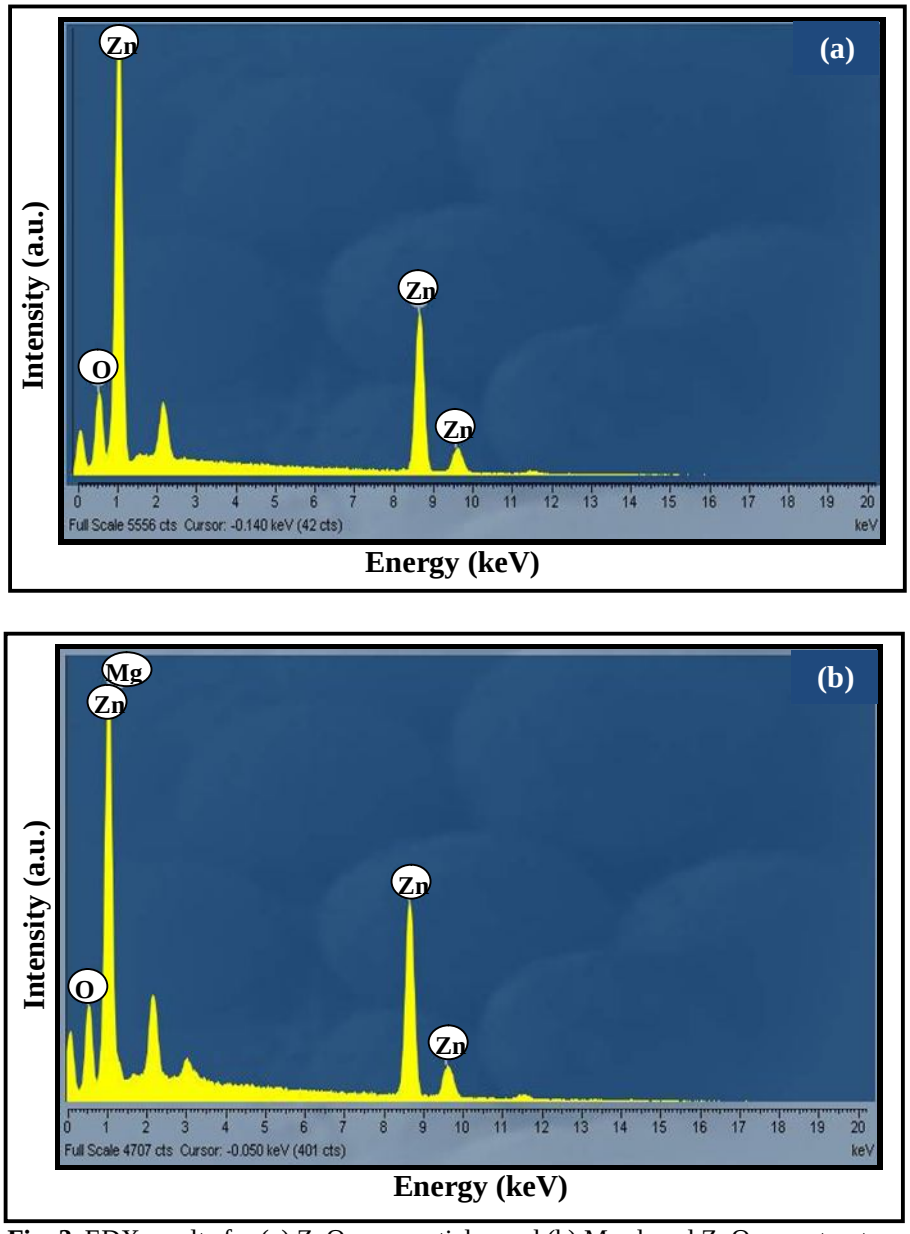

Fig. 3. EDX results for (a) ZnO nanoparticles and (b) Mg-doped ZnO nanostructures.

nanostructures are shown in Fig. S4b. The broad absorption bands in the range of 3100-3600 cm^{-1} correspond to the O-H stretching vibration of adsorbed water molecules on the samples. The peaks at about 560 and 1438 cm^{-1} are related to Zn-O and Mg-O vibrations, respectively [12].

Photocatalytic activities of the prepared samples were investigated by degradation of MB under UV irradiation at 25 ºC. (Fig. 5a). The degradation of MB on Mg-doped ZnO nanostructures takes place at 150 min which is much less than the corresponding time for the undoped ZnO nanoparticles. It is evident that in presence of Mg-doped ZnO nanostructures, without using the light irradiation (dark experiment), about 11% of MB molecules are adsorbed on the Mg-doped nanostructures during 150 min. Moreover, in presence of the light and without using the nanostructures (photolysis experiments), only about 8.3% of MB molecules

are degraded after irradiation for 150 min. Hence, the decrease of MB molecules in the solution containing Mg-doped ZnO nanostructures majorly is related to photocatalytic degradation of them. Plots of absorbance against wavelength for the degradation reaction on the doped ZnO ([MB] = 2.75×10^{-5} M, catalyst weight = 0.1 g, ultrasonic irradiation time = 60 min, calcination temperature = 400 °C, and pH = 5.4) at various irradiation times are shown in Fig. 5b. As can be seen, the absorbance gradually diminishes with increasing the irradiation time. Molecules of MB have two absorption maxima in the visible range. These absorptions correspond to the conjugation system between the two aromatic rings [26,27]. Moreover, the two absorption maxima at the UV range are related to the aromatic rings. During photocatalytic degradation of MB, intermediates such as azures and thionine are formed [28]. These intermediates are degraded to produce benzene sulfonic acid, phenol, and formic acid [29]. Afterwards, the intermediates are degraded to produce final degradation products [30]. As evident from Fig. 5b, during the degradation of MB on the nanostructures, the absorbance at UV and visible ranges decrease with increasing the irradiation time and new absorption bands are not formed. Therefore, it can be concluded that stable intermediates such as azures, thionine, and benzene sulfonic acid, with distinct absorptions in UV and visible ranges, are not formed during the degradation reaction. Furthermore, Fig. 5c shows FT-IR spectra for the fresh and recycled Mg-doped ZnO naostructures. As can be seen, these spectra are very similar to each other. Hence, it can be concluded that after complete degradation of MB on the nanostructures, there is no any adsorption of MB and its intermediates produced during the degradation reaction.

The observed first-order rate constant (k_{obs}) of the degradation reactions was calculated by using $\ln A_0/A = k_{obs}t$, in which A_0 and A are absorbance of the solution in 664 nm before and after irradiation for t min [31]. The rate constants for degradation of MB on the doped and undoped ZnO are 22.6×10^{-3} and 9.17×10^{-3} min^{-1}, respectively. Hence, the degradation rate constant on Mg-doped ZnO nanostructures increases nearly 2.5-fold relative to the undoped one. Very recently, Yousefi *et al*. investigated the effect of Mg doping on photoluminescence (PL) of ZnO nanostructures [32]. The results showed that the intensity of PL spectra in 375 nm decreases by increasing Mg content. It is well known that intensity of PL is related to life time of electron-hole pairs, and doping of Mg on ZnO nanostructures decreases recombination of the charge carriers [33]. In Mg-doped ZnO nanostructures, Mg^{2+} ions act as trapping sites of the charge carriers, which prolongs the lifetime of them. For this reason, the photocatalytic degradation of MB on the doped ZnO is higher than that of the undoped one.

To study the influence of the ultrasonic irradiation time applied for preparation of Mg-doped ZnO nanostructures, four comparative samples were prepared, keeping the reaction parameters constant except that the nanostructures were prepared by irradiations for 30, 60, 90 and 120 min (Fig. 6a). It is clear that the degradation rate constant initially increases with the irradiation time up to 60 min and then decreases. Ultrasonic irradiation time can change crystallinity, size and morphology of nanomaterials [34]. Enhancing the photocatalytic activity with increasing the irradiation time can be attributed to increasing crystallinity of the nanostructures. Figure 6b shows SEM image for the prepared nanostructures by ultrasonic irradiation for 120 min. It is clearly evident that the prepared nanostructures are highly aggregated. Hence, its ability for adsorption of MB molecules decreases. As a result, the photocatalytic activity decreased at higher irradiation times (Fig. 6a).

It is well known that calcination temperature changes photocatalytic activity of nanomaterials [34]. To investigate the effect of calcination temperature, degradation of MB on Mg-doped ZnO nanostructures calcined for 2 h at various temperatures was considered (Fig. 7a). As can be seen, the degradation rate constant increases with calcination temperature up to 400 ºC and then decreases (Fig. 7b). It is accepted that increasing calcination temperature can cause formation of photocatalysts with high crystallinity [35]. Therefore, it is expected that photocatalysts treated at higher temperatures might display better photocatalytic activity. Size of nanomaterials usually increases with increasing the calcination temperature [36]. Decreasing the degradation rate constant at high calcination temperatures can be attributed to the increasing size of the nanostructures and hence decreasing surface area of the catalyst.

In heterogeneous photocatalysis reactions, weight of catalyst has reasonable effect on degradation reaction. Hence, a series of experiments were carried out by changing

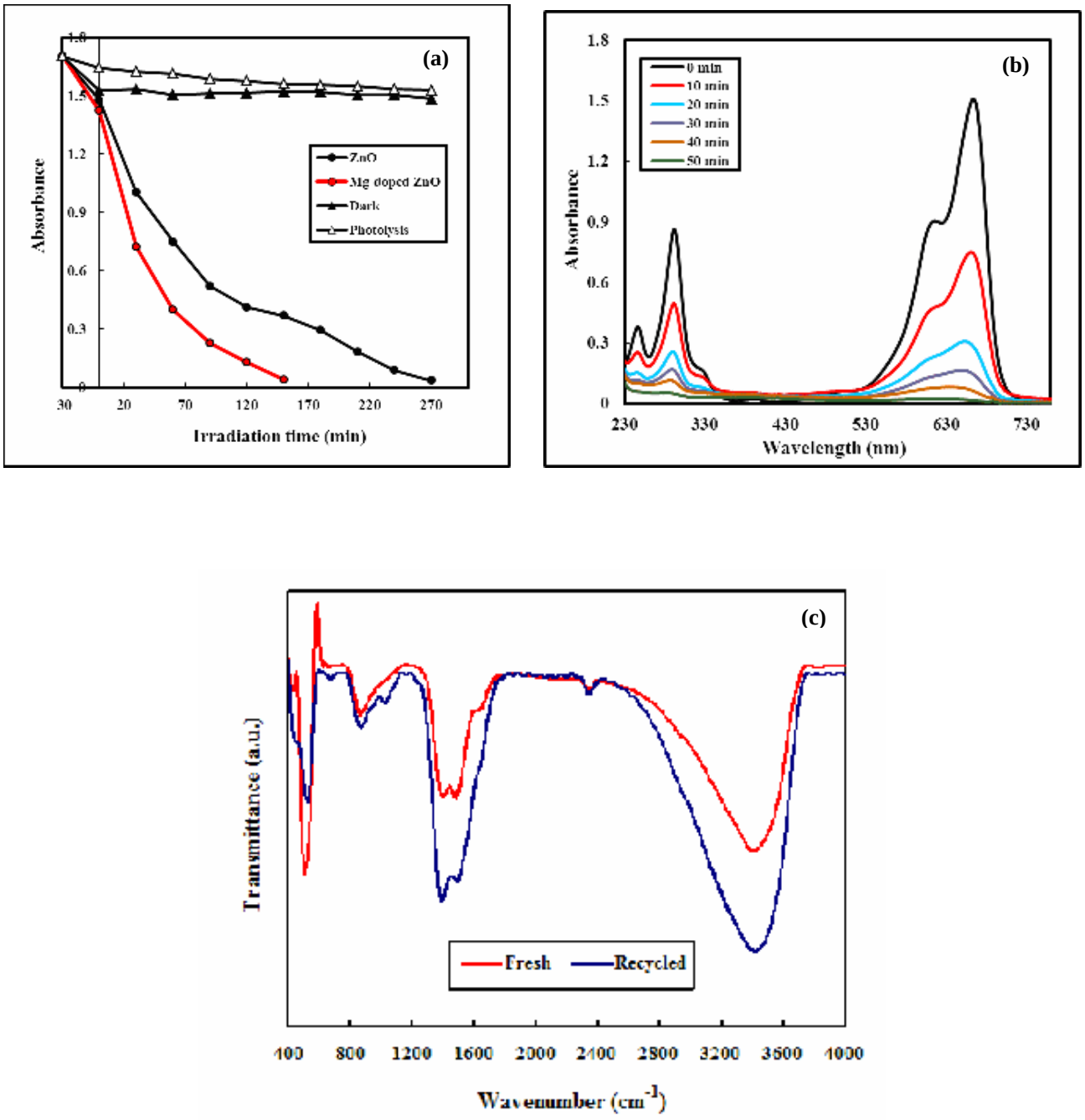

Fig. 5. (a) Photodegradation of MB on ZnO nanoparticles and Mg-doped ZnO nanostructures along with dark and photolysis data. (b) Plots of absorbance againest wavelength for degradation of MB on Mg-doped ZnO nanostructures at various irradiation times. (c) FT-IR spectra for the fresh and recycled Mg-doped ZnO nanostructures.

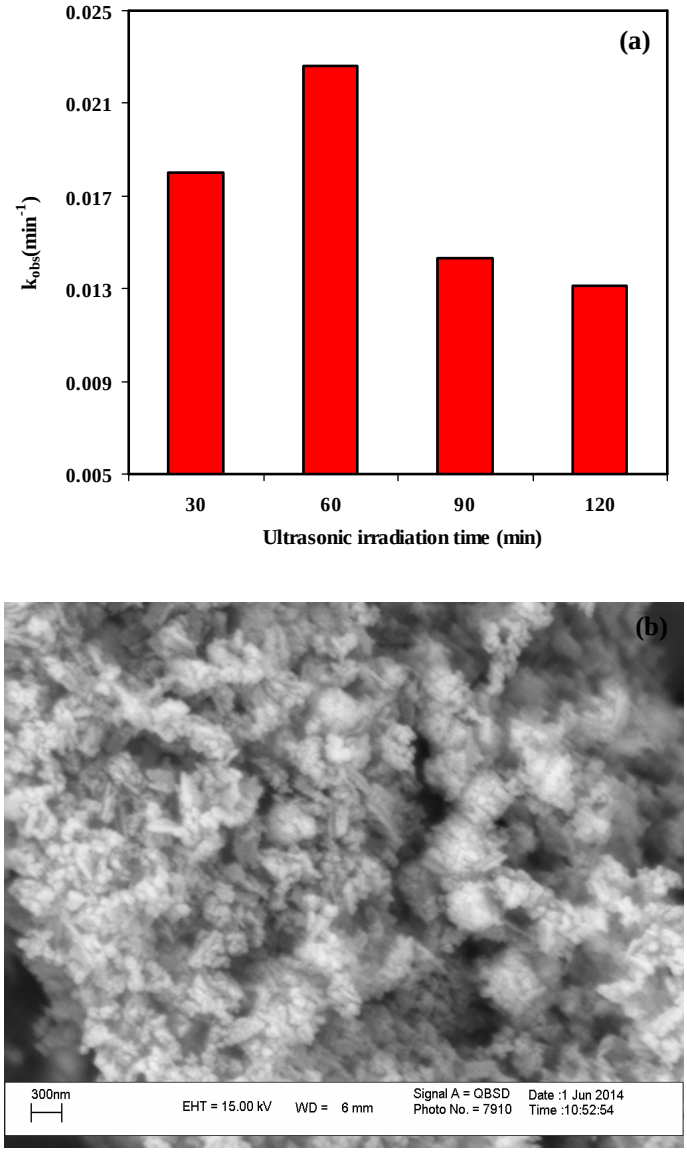

Fig. 6. (a) Photodegradation of MB on the nanostructures prepared at various ultrasonic irradiation times. (b) SEM image for the nanostructures prepared by ultrasonic irradiation for 120 min.

weight of the nanostructures between 0.025 and 0.15 g (Table 1). It is evident that the rate constant increases with weight of the photocatalyst up to 0.1 g and then decreases. With increasing weight of the photocatalyst, the active sites and absorption of the irradiating light are increased. However, more photocatalyst increases scattering of light and reduces the light penetration through the solution [37]. Hence, the degradation rate constant decreases using much greater weight of the catalyst.

It is well known that pH of solutions has remarkable influence on photocatalytic activity. The effects of solution pH on the degradation reaction were studied by varying the initial pH between 2.5 and 12 (Fig. S8a). Similar to ZnO based photocatalysts, decrease of the degradation reaction with decreasing pH of the solution is attributed to dissolution of the nanostructures [38]:

Mg-doped ZnO + $2H^+$ ⟶ Zn^{2+} (along with Mg^{2+}) + H_2O (1)

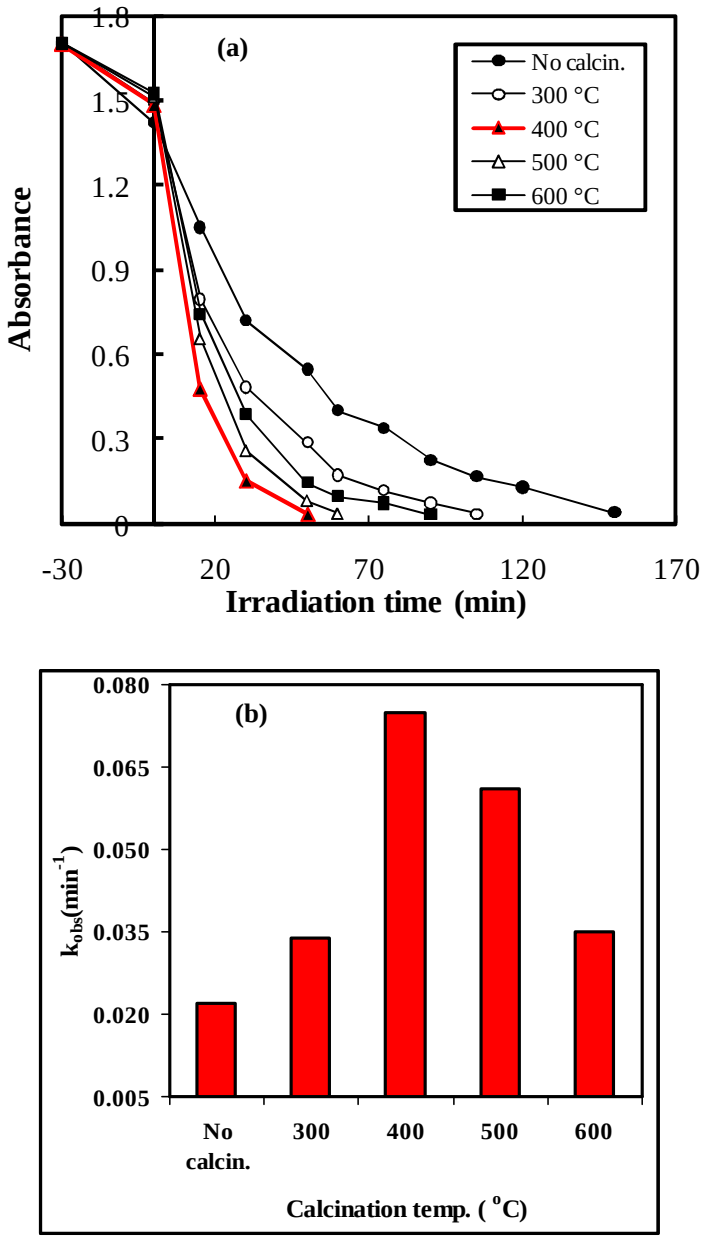

Fig. 7. (a) Photodegradation of MB on the nanostructures calcined at various temperatures. (b) Plot of the rate constant *vs.* calcination temperature.

Hence, because of low stability of the photocatalyst, the degradation reaction is decreased at more acidic solutions. Very recently, photolysis of MB molecules under sunlight irradiation has been reported [39]. The results show that the photolysis reaction rapidly increases in alkaline solutions. Hence, it is necessary to investigate the extent of MB stability under UV irradiation in different solutions. In Fig. S8b, plots for photolysis of MB in solutions with different pH are shown. As can be seen, in solution with pH < 7, photolysis of MB is not noticeable; but the reaction is suddenly increased with increasing pH of the solution. Therefore, because of much greater photolysis, alkaline solutions are not proper solutions for photocatalytic degradation of MB under UV irradiation. At pH 5.4, after

Table 1. Effect of the Nanostructure Weight on the Degradation Rate Constant of MB

No.	Catalyst weight (g)	$k_{obs} \times 10^{-3}$ (min^{-1})
1	0.025	14.9
2	0.050	17.0
3	0.075	19.0
4	0.100	75.0
5	0.150	52.0

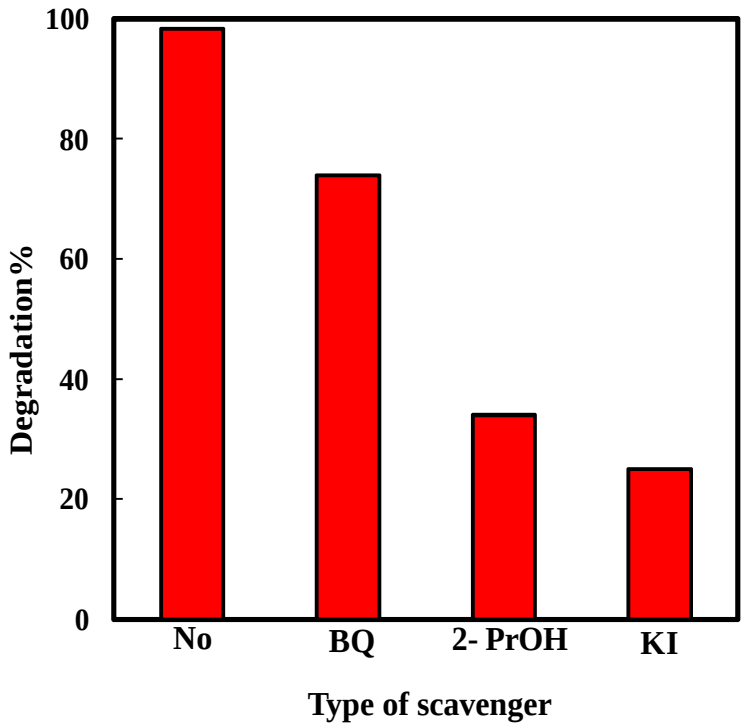

Fig. 9. Plot of %degradation of MB on the nanostructures in presence of various scavengers.

UV irradiation for 25 min, only about 3% of MB molecules were degraded by photolysis reaction. As evident in Fig. S8b, in presence of Mg-doped ZnO nanostructures, MB molecules are completely disappeared at 25 min. Hence, this solution is proper for photocatalytic degradation of MB on the nanostructures under UV irradiation.

To determine the role of the reactive species on the degradation reaction, effects of various scavengers with 1.0 mM on the degradation reaction was investigated after irradiation for 50 min and the results are shown in Fig. 9. Without using any scavenger, the degradation efficiency is 98.4%. By using benzoquinone (scavenger for $^{\bullet}O_2^-$), 2-PrOH

(scavenger for °OH), and KI (scavenger for hole) [40,41], the degradation efficiency decreases to 74, 34 and 25%, respectively. Decrease of the degradation efficiency in presence of KI and 2-PrOH is greater than that of benzoquinone. Hence, it can be concluded that the role of the holes and hydroxyl radicals in degradation of MB is greater than supper oxide ions.

CONCLUSIONS

Ultrasonic irradiation method was applied for preparation of Mg-doped ZnO nanostructures in water and the prepared samples were fairly characterized by different techniques. The rate constants for degradation of MB on the doped and undoped ZnO are 22.6×10^{-3} and 9.17×10^{-3} min^{-1}, respectively. Photocatalytic activity of the nanostructures shows the best results for the prepared sample using ultrasonic irradiation for 60 min. The degradation rate constant increases with increasing calcination temperature up to 400 °C and then decreases. At pH 5.4 (as an optimum solution), after UV irradiation for 25 min, only about 3% of MB molecules are degrade by photolysis reaction and MB molecules are completely degraded on Mg-doped ZnO nanostructures. In presence of benzoquinone, 2-PrOH and KI, the degradation efficiency decreases to 74, 34, and 25%, respectively. Therefore, it can be concluded that the holes and hydroxyl radicals play a vital role in degradation of MB relative to superoxide ions.

ACKNOWLEDGMENTS

The authors wish to acknowledge University of Mohaghegh Ardabili, for financial support of this work.

REFERENCES

[1] M.Y. Masoomi, G. Mahmoudi, A. Morsali, J. Coordination Chem. 63 (2010) 1186.

[2] M.Y. Masoomi, A. Morsali, Coordination Chem. Rev. 256 (2012) 2921.

[3] M.Y. Masoomi, A. Morsali, RSC Adv. 3 (2013) 19191.

[4] E. Grabowska, J. Reszczynska, A. Zaleska, Water Res. 46 (2012) 5453.

[5] S.-M. Lam, J.-C. Sin, A.Z. Abdullah, A.R. Mohamed, Desalin. Water Treatment 41 (2012) 131.

[6] L. Zhanga, H.H. Mohamed, R. Dillert, D. Bahnemann, J. Photochem. Photobiol. C: Photochem. Rev. 13 (2012) 2636.

[7] H.H. Mohamed, D.W. Bahnemann, Appl. Catal. B: Environ. 128 (2012) 91.

[8] P.R. Potti, V.C. Srivastava, Mater. Sci. Forum 757 (2013) 165.

[9] X. Qiu, L. Li, J. Zheng, J. Liu, X. Sun, G. Li, J. Phys. Chem. C 112 (2008) 12242.

[10] S. Sundar Manoharan, S. Arora, Mater. Sci. Eng. B 162 (2009) 68.

[11] M. Sharma, P. Jeevanandam, Superlatt. Microstruct. 52 (2012) 1083.

[12] V. Etacheri, R. Roshan, V. Kumar, ACS Appl. Mater. Interfaces 4 (2012) 2717.

[13] Q. Shi, J. Zhang, D. Zhang, C. Wang, B. Yang, B. Zhang, W. Wang, Mater. Sci. Eng. B 177 (2012) 689.

[14] R. Yousefi, A. Khorsand Zak, F. Jamali-Sheini, Mater. Sci. Semiconductor Process 16 (2013) 771.

[15] H. Nouri, A. Habibi-Yangjeh, Adv. Powder Technol. 25 (2014) 1016.

[16] I.A. Siddiquey, T. Furusawa, M. Sato, N.M. Bahadur, M.M. Alam, N. Suzuki, Ultrasonic Sonochem. 19 (2012) 750.

[17] D. Xie, L. Chang, F. Wang, G. Du, B. Xu, J. Alloys Compd. 545 (2012) 176.

[18] J.-F. Zhou, J. Ao, Y.-Y. Xia, H.-M. Xiong, J. Colloid Interf. Sci. 393 (2013) 80.

[19] D. Chen, K. Wang, D. Xiang, R. Zong, W. Yao, Y. Zhu, Appl. Catal. B: Environ. 147 (2014) 554.

[20] H.-M. Xiong, D.G. Shchukin, H. Mohwald, Y. Xu, Y.-Y. Xia, Angew. Chem. Int. Ed. 48 (2009) 2727.

[21] X. Lu, Z. Liu, Y. Zhu, L. Jiang, Mater. Res. Bull. 46 (2011) 1638.

[22] M.H. Entezari, P. Kruus, Ultrason. Sonochem. 1 (1994) S75.

[23] B.G. Mishra, G.R. Rao, J. Mol. Catal. A: Chem. 243 (2006) 204.

[24] S. Sharma, R. Vyas, N. Sharma, V. Singh, A. Singh, V. Kataria, B.K. Gupta, Y.K. Vijay, J. Alloys Compd. 552 (2013) 208.

[25] L.I. Berger, Semiconductor materials, CRC, Boca

Raton, 1997.

[26] A.E.H. Machado, J.A. de Miranda, R.F. de Freitas, E.T.F.M. Duarte, L.F. Ferreira, Y.D.T. Albuquerque, R. Ruggiero, C. Sattler, L. de Oliveira, J. Photochem. Photobiol. A: Chem. 155 (2003) 231.

[27] C. Yogi, K. Kojima, N. Wada, H. Tokumoto, T. Takai, T. Mizoguchi, H. Tamiaki, Thin Solid Films 516 (2008) 5881.

[28] M.A. Rauf, M.A. Meetani, A. Khaleel, A. Ahmed, Chem. Eng. J. 157 (2010) 373.

[29] C. Wen, Y.-J. Zhu, T. Kanbara, H.-Z. Zhu, C.-F. Xiao, Desalination 249 (2009) 621.

[30] Z. Yu, S.S.C. Chuang, Appl. Catal. B: Environ. 83 (2008) 277.

[31] M. Pirhashemi, A. Habibi-Yangjeh, Appl. Surf. Sci. 283 (2013) 1080.

[32] R. Yousefi, A. Khorsand Zak, F. Jamali-Sheini, Mater. Sci. Semicond. Proc. 16 (2013) 771.

[33] Y. Zang, L. Li, X. Li, R. Lin, G. Li, Chem. Eng. J. 246 (2014) 277.

[34] M. Pirhashemi, A. Habibi-Yangjeh, J. Alloys Compd. 601 (2014) 1.

[35] M.V. Shankar, S. Anandan, N. Venkatachalam, B. Arabindoo, V. Murugesan, J. Chem. Technol. Biotechnol. 79 (2004) 1279.

[36] S.Y. Kim, T.H. Lim, T.S. Chang, C.H. Shin, Catal. Lett. 117 (2007) 112.

[37] H. Kisch, Angew. Chem. Int. Ed. 51 (2012) 2.

[38] N. Sobana, M. Swaminathan, Sep. Purif. Technol. 56 (2007) 101.

[39] T. Soltani, M.H. Entezari, J. Mol. Catal. A: Chem. 377 (2013) 197.

[40] G.T. Li, K.H. Wong, X.W. Zhang, C. Hu, J.C. Yu, R.C.Y. Chan, P.K. Wong, Chemosphere 76 (2009) 1185.

[41] L.S. Zhang, K.H. Wong, H.Y. Yip, C. Hu, J.C. Yu, C.Y. Chan, P.K. Wong, Environ. Sci. Technol. 44 (2010) 1392.